RADIATION EFFECTS & DEFECTS IN SOLIDS
2018, VOL. 173, NOS. 5–6, 474–488
https://doi.org/10.1080/10420150.2018.1477155

Taylor & Francis
Taylor & Francis Group

Measurement of photon interaction parameters of high-performance polymers and their composites

M. Büyükyıldız[a]*, M. A. Taşdelen [b], Y. Karabul[c], M. Çağlar[c,d], O. İçelli[c] and E. Boydaş[e]

[a]Faculty of Engineering, Yalova University, Yalova, Turkey; [b]Faculty of Engineering, Department of Polymer Engineering, Yalova University, Yalova, Turkey; [c]Faculty of Arts and Science, Department of Physics, Yıldız Technical University, İstanbul, Turkey; [d]Institute of Health Sciences, Department of Medical Physics, Istanbul Medipol University, İstanbul, Turkey; [e]Faculty of Science, Department of Physics, Atatürk University, Erzurum, Turkey

ABSTRACT

In the present study, commercially important high-performance polymers and their composites have been investigated with respect to photon interactions as means of mass attenuation coefficient (μ/ρ), mean free path (MFP), half-value layer (HVL), effective atomic number (Z_{eff}), effective electron density (N_{eff}), and energy absorption and exposure buildup factors (EABF and EBF) at different photon energies. For this purpose, sample plates were prepared by extrusion and injection techniques using polyethersulfone, polyetherimide, acrylonitrile butadiene styrene copolymer, polyamide 66, polyphthalamide, and polypropylene copolymers as high-performance polymers and glass and carbon fibers as reinforcement. The (μ/ρ)s of the materials were measured at 81 and 356 keV photon energies to determine MFP, HVL, Z_{eff}, and N_{eff}. The theoretical values of these parameters were calculated via ZXCOM, WinXCom and Monte Carlo N-Particle simulation code (MCNP), and a good agreement was obtained between WinXCom–MCNP and MCNP–Exp. Finally, EABFs and EBFs of the samples were calculated up to around 40 MFP in the energy region 0.015–15 MeV and significant variations were observed in the continuous energy and MFP regions.

ARTICLE HISTORY
Received 18 September 2017
Accepted 2 May 2018

KEYWORDS
Effective atomic number; high-performance polymer; mass attenuation coefficient; buildup factor; ZXCOM; MCNP

1. Introduction

Today, high-performance polymers (HPP) are widely used in many applications such as automotive, medicine, and electronics due to their high stiffness, suitable dimensional and chemical stability, and favorable thermal and dielectric properties. Furthermore, the metals used in transportation industries are replaced with them to reduce weight and improve fuel efficiency (*1*). Similarly, in the fields of medicine, nuclear physics, radiation and airspace, the manufacturers are looking for solutions to protect the users against the X and/or gamma rays (*2, 3*). In this line, HPP plays an important role particularly in shielding, as they can easily be reinforced with inorganic particles and fibers to protect the rays as discussed above.

CONTACT M. Büyükyıldız m.buyukyildiz@gmail.com
*Present address: Termal Vocational School, Yalova University, 77400 Yalova, Turkey

There are some studies for polymers in terms of radiation and shielding applications in the literature. The high-density polyethylene reinforced with natural fiber and lead oxide composites were investigated for fast neutron and gamma-ray interactions and the materials offered sufficient radiation attenuation properties (*4*). Epoxy/ilmenite (titanium-iron oxide mineral) composites were also studied for neutrons and gamma ray attenuation and the results of mass attenuation coefficients were compared with the theoretical values from XCOM program, and the authors found a reasonable agreement between experimental and theoretical results (*5*). In another study, Epoxy/ Pb_3O_4 (epoxy/trilead tetroxide) composites were prepared by Eid et al. to protect public and personnel from the effect of scattered radiation during radiotherapy (*6*). They reported that the composites were efficient in the range of 660 to 1371 keV. Korkut et al. produced epoxy-ferrochromium slag composites for X-ray, gamma-ray and neutron particle interactions and showed that radiation shielding performance increased with increasing ferrochromium slag additive in epoxy (*7*). Aygün et al. (*8*) produced Epoxy/Molybdenum composites and tested their neutron-shielding capacities. In addition, they used FLUKA and GEANT4 Monte Carlo (MC) programs for theoretical values and the results were compared with some shielding materials. Epoxy polymers reinforced with cement, aluminum, and lead were also studied in terms of linear attenuation coefficient and buildup factor for radiation shielding using 0.662 MeV gamma rays emitted from the radioactive Cs-137 source (*9*). The results were evaluated via concentration of high elements in the composites. Isophthalic-Bi_2O_3 polymer composites fabricated by open mold cast technique were investigated to determine their gamma-ray attenuation parameters such as linear attenuation coefficient and half-value-layer (HVL) (*10*). Although the metals are well-known shielding materials, they have various drawbacks such as susceptibility to corrosion, harsh operating and environmental conditions. To overcome these limitations, several polymers and their composites can be used as shielding materials instead of metals. Sathiyaraj et al. (*11*) studied effective atomic number and buildup factors of metal nano particle doped polymer gel and obtained some important results for shielding applications. Kurudirek investigated shielding properties of borate glasses for gamma, neutron and charged particle radiations, and compared the results for the type of radiations (*12*).

To explore the possible applications of HPP, their relevant shielding parameters against X and/or gamma have to be determined initially. In the present study, the radiation interaction parameters such as μ/ρ, MFP, HVL, Z_{eff}, N_{eff}, EBF, and EABF of the commercially important high-performance polymers and their composites were intensively investigated. The motivation for this study comes from the fact that these parameters are highly important in designing materials that are used in radiation and shielding applications. To this end, the polymeric plates were prepared with polyethersulfone, polyetherimide, acrylonitrile butadiene styrene copolymer, polyamide 66, polyphthalamide, and polypropylene copolymer and their composites containing carbon and glass fibers with different ratio using extrusion and subsequent injection.

2. Method

2.1. The mass attenuation coefficients

The mass attenuation coefficient of compound or mixture can be obtained by the Beer–Lambert law at any monoenergetic photon by using the following equation.

$$I = I_0 e^{-\mu x} = I_0 e^{-\mu_m t}, \tag{1}$$

$$\mu_m = \left(\frac{\mu}{\rho}\right) = \frac{\ln(I_0/I)}{\rho t}, \tag{2}$$

where I and I_0 are attenuated and unattenuated photon intensities, μ (cm^{-1}) and μ_m (cm^2g^{-1}) are linear and mass attenuation coefficients, t (gcm^{-2}) and x (cm) are the mass thickness (the mass per unit area), and thickness and ρ (gcm^{-3}) is the density of material as seen in Table 1.

The total mass attenuation coefficient μ_m for any composite of elements is given by mixture rule:

$$\mu_m = \left(\frac{\mu}{\rho}\right) = \sum_i w_i(\mu/\rho)_i, \tag{3}$$

w_i is ith constituent element $w_i = n_iA_i/\sum_i n_iA_i$, in the equation, A_i is the atomic weight of the ith element, and n_i is the number of atoms of ith constituent element in the composite. Moreover, the composition of polymers via WDXRF spectrometer is given in Table 2. For determination of total atomic cross section or theoretical mass attenuation coefficients, WinXCom computer program was utilized (*13*). The experimental, theoretical and simulation results are given in Table 3. Half-value layer (HVL) is the thickness of the material at which the intensity of radiation entering by one-half and mean free path (MFP) is the average distance between two successive interactions. In Table 4, the values have been calculated using the linear attenuation coefficient (μ) according to the following equations:

$$\text{HVL} = \frac{\ln(2)}{\mu} = \frac{0.693}{\mu} \quad \text{and} \quad \text{MFP} = \frac{1}{\mu}. \tag{4}$$

2.2. Effective atomic number

The total photon interaction cross section (σ_t) for materials can be obtained from the measured mass attenuation coefficients μ_m using the following equation:

$$\sigma_t = \frac{\mu_m \sum_i n_iA_i}{N_A}. \tag{5}$$

Table 1. Formulas and densities of the given polymers.

Polymer		Content	density (g/cm3)
P1	Tecotek (PESU)	Unfilled polyethersulfone	1.37
P2	Tecotek (EI20 NL PEI)	Unfilled polyetherimide	1.27
P3	Tecotek (AB40 NL ABS)	Unfilled acrylonitrile butadiene styrene copolymer	1.05
P4	Tecotek (PC40 NL PC)	Unfilled polycarbonate	1.19
P5	Tecotek (AB40 HF55 NL)	Acrylonitrile butadiene styrene (45%) + 150 µm Copper powder (55%)	2.01
P6	Tecolen (CP20 HF75 NL IM)	Polypropylene copolymer (15%) + Iron oxide powder (75%) + Impact modifier (QUEO 8210, 10%)	2.24
P7	Tecopeak (PK40 NL)	Unfilled Polyether ether ketone	1.30
P8	Tecomid (NA30 CR30 BK111 TC)	Polyamide 66 (70%) + carbon fiber (AKSACA AC 04-01, 30%)	1.27
P9	Tecomid (NT40 KC60 NL HS OA)	Polyphthalamide (40%) + chopped carbon fiber (30%)+ chopped glass fiber (30%)	1.61
P10	Tecomid (NT40 GD60 NL HS)	Polyphthalamide (40%) + chopped glass fiber (60%)	1.75
P11	Tecomid (NT40 NL)	Unfilled polyphthalamide	1.20
P12	Tecomid (NA40 CN20 BK012 HS)	Polyamide 66 (80%) + Nickel coated carbon fiber (20%)	1.28
P13	Tecomid (NT40 KC50 NL HS OB)	Polyphthalamide (50%) + chopped carbon fiber (20%)+ chopped glass fiber (30%)	1.49

Table 2. Chemical composition of the investigated polymers from WDXRF.

	P1	P2	P3	P4	P5	P6	P7	P8	P9	P10	P11	P12	P13
B	2.634	1.332											0.674
C	58.365	80.309	98.778	80.536	86.995	73.478	82.168	56.991	70.550	65.490	71.095	68.817	72.352
N					7.233			12.702	10.767	11.212	14.338	14.653	11.317
O	23.066	17.623	1.060	19.422	3.887	20.630	17.757	22.199	13.667	14.259	14.528	14.876	12.807
Na		0.124	0.017	0.020	0.067	0.058	0.030	0.035	0.096	0.063		0.014	0.054
Mg		0.008	0.023			0.093	0.003		0.028	0.087		0.002	
Al		0.007		0.002	0.008	0.052	0.002	1.775	0.606	1.196	0.003	0.003	0.314
Si		0.012	0.073	0.005	0.014	0.080	0.007	0.018	2.078	4.144	0.006	0.008	1.087
P	0.004	0.001		0.004	0.014	0.006	0.001	6.100	0.003	0.007	0.003	0.006	0.002
S	15.431	0.383	0.044	0.002	0.060	0.007	0.016	0.011	0.004	0.004	0.002	0.001	0.002
Cl	0.470	0.191		0.005	0.015		0.007	0.020	0.011	0.009		0.004	0.008
K	0.030	0.007	0.004		0.005	0.006	0.002	0.005	0.050	0.040	0.021		0.047
Ca		0.003			0.020	0.016	0.004	0.034	2.098	3.434		0.021	1.307
Ti						0.032			0.016	0.025			0.009
V						0.035							
Mn						0.004							
Fe				0.002	0.002	5.502	0.001		0.012	0.012		0.001	0.007
Ni						0.001						1.593	
Cu					1.660				0.001	0.002	0.001		0.002
Zn			0.001	0.003			0.003	0.109			0.001		0.001
Br								0.002	0.008	0.007	0.004		0.008
Sr									0.006	0.007			0.003
Y										0.000			
Zr									0.001	0.001			0.000
Ag		0.001											
Hf					0.021								

Table 3. Mass attenuation coefficients of the given polymers at 81 and 356 keV photon energies.

	81 keV			356 keV		
	Exp.	Th.	MC	Exp.	Th.	MC
	$\mu/\rho(cm^2/g)$					
P1	0.165	0.177	0.174	0.094	0.100	0.099
P2	0.152	0.162	0.162	0.095	0.100	0.099
P3	0.151	0.161	0.159	0.095	0.100	0.099
P4	0.153	0.162	0.161	0.095	0.100	0.099
P5	0.163	0.172	0.170	0.096	0.100	0.100
P6	0.175	0.185	0.186	0.095	0.100	0.099
P7	0.151	0.162	0.160	0.095	0.100	0.099
P8	0.159	0.168	0.165	0.096	0.100	0.099
P9	0.159	0.168	0.168	0.096	0.100	0.100
P10	0.162	0.172	0.169	0.096	0.100	0.100
P11	0.151	0.162	0.161	0.095	0.100	0.099
P12	0.160	0.171	0.169	0.095	0.100	0.100
P13	0.155	0.165	0.165	0.095	0.100	0.099

Here N_A is the Avogadro number and μ_m is the total mass attenuation coefficient of a material. In addition, the total atomic (σ_a) and electronic (σ_e) cross sections can be calculated by the formulas given below:

$$\sigma_a = \frac{\sigma_t}{\sum_i n_i} \quad \text{and} \quad \sigma_e = \frac{1}{N_A} \sum \frac{f_i A_i}{Z_i} (\mu_m)_i, \tag{6}$$

Table 4. MFPs and HVLs of the given polymers at 81 and 356 keV photon energies.

	81 keV			356 keV			81 keV			356 keV		
	Exp.	Th.	Dif.%	Exp.	Th.	Dif.%	Exp.	Th.	Dif.%	Exp.	Th.	Dif.%
	MFP						HVL					
P1	4.419	4.132	6.86	7.740	7.277	6.36	3.061	2.864	6.86	5.365	5.044	6.36
P2	5.178	4.858	6.58	8.325	7.884	5.59	3.589	3.368	6.58	5.770	5.464	5.59
P3	6.323	5.929	6.64	10.031	9.529	5.27	4.383	4.110	6.64	6.953	6.605	5.27
P4	5.501	5.195	5.89	8.855	8.405	5.36	3.813	3.601	5.89	6.138	5.826	5.36
P5	3.049	2.890	5.52	5.183	4.975	4.17	2.113	2.003	5.52	3.592	3.449	4.17
P6	2.549	2.411	5.71	4.694	4.465	5.13	1.767	1.671	5.71	3.254	3.095	5.13
P7	5.089	4.758	6.93	8.090	7.694	5.15	3.526	3.298	6.93	5.608	5.333	5.15
P8	4.952	4.687	5.66	8.214	7.885	4.17	3.433	3.249	5.66	5.694	5.466	4.17
P9	3.915	3.705	5.67	6.504	6.208	4.76	2.714	2.568	5.67	4.508	4.303	4.76
P10	3.531	3.325	6.18	5.983	5.709	4.82	2.447	2.305	6.18	4.147	3.957	4.82
P11	5.504	5.147	6.94	8.810	8.334	5.71	3.816	3.568	6.94	6.107	5.777	5.71
P12	4.894	4.578	6.89	8.236	7.808	5.48	3.392	3.173	6.89	5.709	5.412	5.48
P13	4.326	4.064	6.45	7.089	6.713	5.60	2.999	2.817	6.45	4.914	4.653	5.60
Ordinary				4.305								
Hematite–serpentine				3.922								
Ilmentite–limonite				3.448								
Basalt–magnetite				3.247								
Ilmenite				2.860								

where Z_i is the atomic number for the ith element and f_i is the fractional abundance of the ith element with respect to a number of atoms. Also, effective atomic number, total atomic and electronic cross sections can be obtained through the following relation:

$$Z_{eff} = \frac{\sigma_a}{\sigma_e}. \tag{7}$$

Following this, effective electron densities (number of electrons per unit mass, N_{eff}) of the materials can be calculated through the formula below:

$$N_{eff} = N_A \frac{nZ_{eff}}{\sum_i n_i A_i} = \frac{Z_{eff}}{\langle \text{A} \rangle} (\text{electrons}/g), \tag{8}$$

where $\langle A \rangle$ is the average atomic mass of materials.

The effective atomic number and electron density results are given in Table 5. The buildup factors of the multi-element materials were calculated by the well-known G–P fitting method as mentioned previously by different authors (*14*–*17*).

On the other hand, ZXCOM computer program was used to calculate Z_{eff}'s of the polymers at the investigated photon energies from 1 to 180 scattering degree (*18*). This program uses the Rayleigh and Compton scattering of photons in order to calculate Z_{eff} of numerous composites at various momentum transfer, which depends on energy and scattering angle. In addition, MC method can be used to precisely simulate the radiation transfer and has been in practice for more than half of a century (*19*). MC user codes that simulate radiation phenomena presently exist. MCNP is a common purpose MC, N-Particle user code managed by Los Alamos National Laboratory. In this study, we used an MCNP-5 simulation package. Firstly, NaI(Tl) detector was drawn and then collimated with pure lead. A narrow beam setup was used to detect the incident and transmit photon energies. It was simulated with a spherical source (radius 0.2 cm) to match theoretical results. The source was modeled

Table 5. Zeffs and Neffs of the given polymers at 81 and 356 keV photon energies.

	81 keV			356 keV			81 keV		356 keV	
	Zeff						Neff			
	Exp.	Th.	Dif.%	Exp.	Th.	Dif.%	Exp.	Th.	Exp.	Th.
P1	7.14	7.59	6.01	6.70	7.12	5.79	2.67	2.84	2.51	2.66
P2	5.97	6.34	5.79	5.96	6.31	5.43	2.80	2.97	2.80	2.96
P3	5.16	5.49	6.03	5.17	5.45	5.15	2.85	3.03	2.86	3.01
P4	5.54	5.84	5.05	5.50	5.79	4.93	2.82	2.97	2.80	2.95
P5	6.31	6.62	4.72	5.98	6.23	4.13	2.87	3.01	2.72	2.83
P6	7.12	7.47	4.78	6.34	6.66	4.82	2.80	2.94	2.49	2.62
P7	5.91	6.31	6.32	5.98	6.30	5.05	2.80	2.98	2.83	2.98
P8	6.71	7.03	4.60	6.57	6.83	3.83	2.76	2.89	2.70	2.81
P9	6.43	6.75	4.76	6.25	6.55	4.55	2.80	2.94	2.72	2.85
P10	6.71	7.07	5.03	6.44	6.74	4.47	2.75	2.90	2.64	2.77
P11	5.99	6.40	6.38	6.03	6.38	5.57	2.80	2.99	2.81	2.98
P12	6.40	6.79	5.71	6.14	6.48	5.27	2.82	2.99	2.71	2.86
P13	6.20	6.56	5.54	6.09	6.44	5.42	2.79	2.96	2.74	2.90

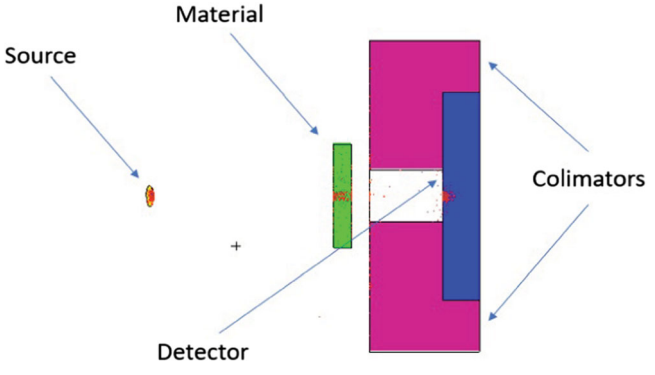

Figure 1. The schematic view of the experimental design for Monte Carlo method.

with two different energies (81 keV and 356 keV) and photons were only directed to a detector (to minimize scatter). Twenty-six different simulations were run by placing the related materials between the source and the detector. Each simulation was performed using 10^6 NPS (Number of Particles) and was evaluated using the statistical significance of $p < .005$. The schematic view of the experimental design is shown in Figure 1.

3. Experimental

For radiation experimental arrangement, all materials were prepared as a plate ($5 \times 50 \times 100$ mm) in Eurotec, after each plate was cut into a sample with 0.9–1.1 mm thickness and 1.5×1.5 cm surface area to measure the radiation interaction parameters. All sample surfaces were polished to obtain maximum photon detection. Finally, transmission operation was carried out to get attenuation coefficients.

The experimental arrangement is displayed in Figure 2. In order to obtain attenuated and unattenuated intensities, all materials were irradiated using 81 and 356 keV gamma rays emitted from a Ba-133 point radioactive source (0.05 μCi). The attenuated and unattenuated peaks emitted from the targets were detected by a $3'' \times 3''$ NaI(Tl) detector (model

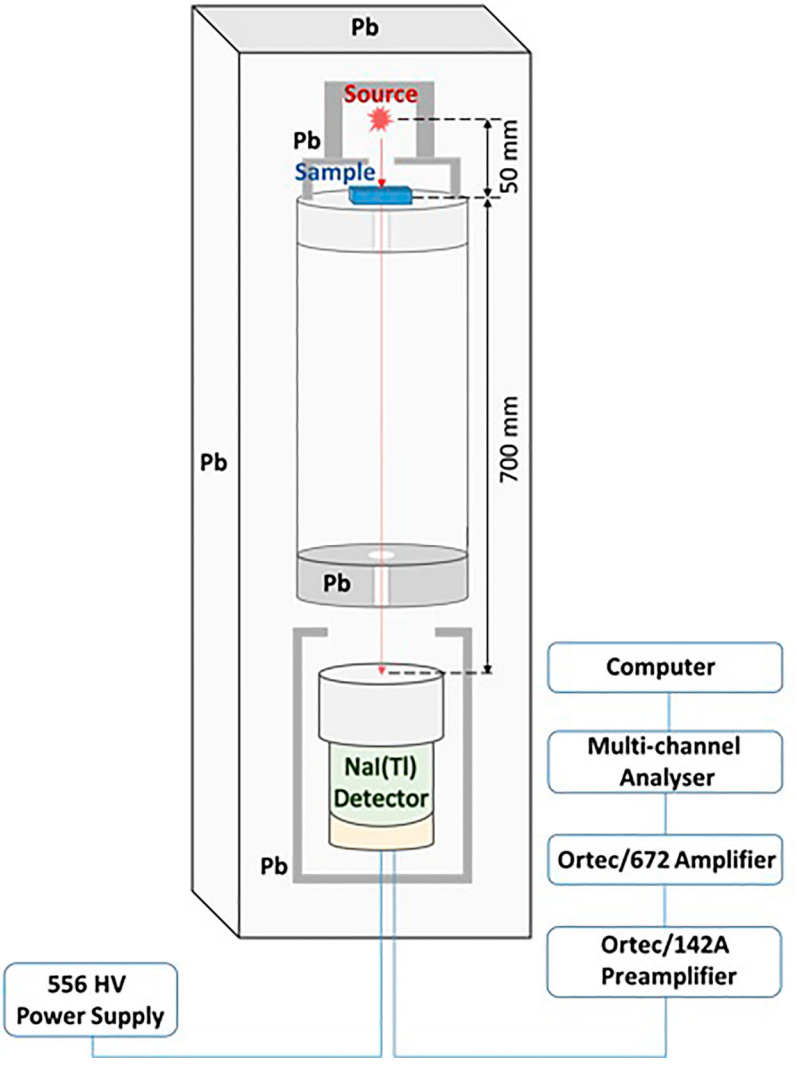

Figure 2. The experimental arrangement for transmission geometry.

905 Ortec-Ametek). The photomultiplier tube (PMT) base, digiBASE (Ortec), had dimensions: 6.3 cm of diameter and 8.0 cm of length, respectively. The FWHM was equal to 46 keV at 662 keV and 65 keV at 1330 keV. The data which were analyzed with the Maestro software collected into 2048 channels of the MCA. A representative spectrum of 81 and 356 keV gamma rays scattered from a Ba-133 point radioactive source for both attenuated and unattenuated intensities is shown in Figure 3.

4. Results and discussion

The symbols and densities of the materials are presented in Table 1. The polymers include B, C, N, O, Na, Mg, Al, Si, P, S, Cl, K, Ca, Ti, V, Mn, Fe, Ni, Cu, Zn, Br, Sr, Zr, Ag, and Hf elements as seen in WDXRF spectra of the samples (Table 2). According to the analysis, all samples

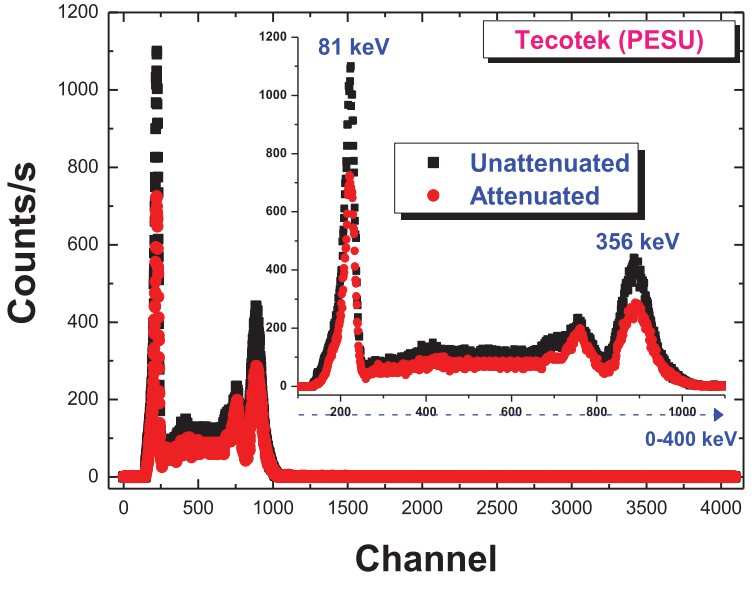

Figure 3. The spectrum of 81 and 356 keV gamma rays for both attenuated and unattenuated intensities.

have pure basic character carbon content between 58% and 98%. As can be seen, the most common elements found in the materials were C, O, and S. The Fe contents of P6 are higher than the other samples. It was found that the shielding properties of the samples raised proportionally by increasing Fe contents.

The mass attenuation coefficient of a material is a measure of the relative dominance of various interactions including photoelectric absorption, Compton scattering, and pair production. As the photoelectric effect dominates below and pair production dominates above 1 MeV, the Compton scattering dominates at 1 MeV (*20*). On the other hand, there was a relative difference (%) [diff.% $= |(A - B)/A| * 100$] among the experimental, theoretical and simulation values of (μ/ρ)s of the materials. Good agreements were observed between Exp.–Th. ($\leq$6.80 and $\leq$5.98), MC–Th. ($\leq$2.04 and $\leq$1.12), and MC–Exp. ($\leq$3.50 and $\leq$3.17) for 81 and 356 keV photon energies, respectively. In order to show the energy dependence of the radiation interaction parameters, low (81 keV) and high (356 keV) photon energies were used to measure the parameters in the study. In this light, significant differences were observed in experimental results (Exp.–Exp.) of (μ/ρ)s (37.09% $\leq$ diff. $\leq$ 45.71%) between 81 and 356 keV energies for all materials. Furthermore, as the total mass attenuation coefficient is highest for P6, the half-value thickness has the lowest value. Density performs a significant role in selecting a shielding material. In addition, the computed values of the linear attenuation coefficients were divided by the density of the samples. The mass attenuation coefficient is more useful than linear attenuation coefficient because it takes into account phase difference. The obtained values of MFP and HVL for 81 keV and 356 keV were given in Table 4. From the table, good agreements in the values of MFP and HVL were found between Exp. and Th. for gamma energies (diff $\leq$ 6.94% for both HVL and MFP). And the investigated materials have values of MFP close to the some important concretes especially P6.

Based on the boron-containing group of P1, P2, and P13, the P1 sample contains more boron element than others. Furthermore, the P1 sample has highest total mass attenuation coefficient and lowest half-value thickness compared to P2 and P13 samples. As a result, the boron contents plays a significant role in increasing the shielding property of

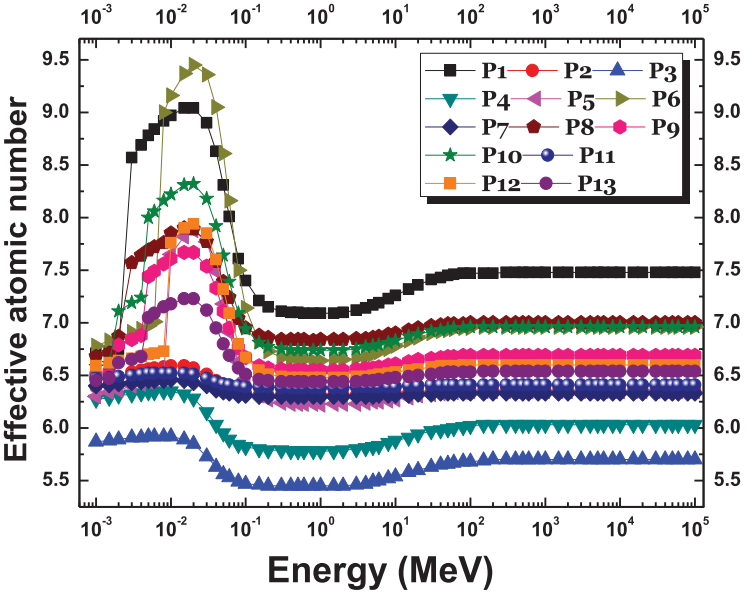

Figure 4. The variation in effective atomic numbers of the polymers.

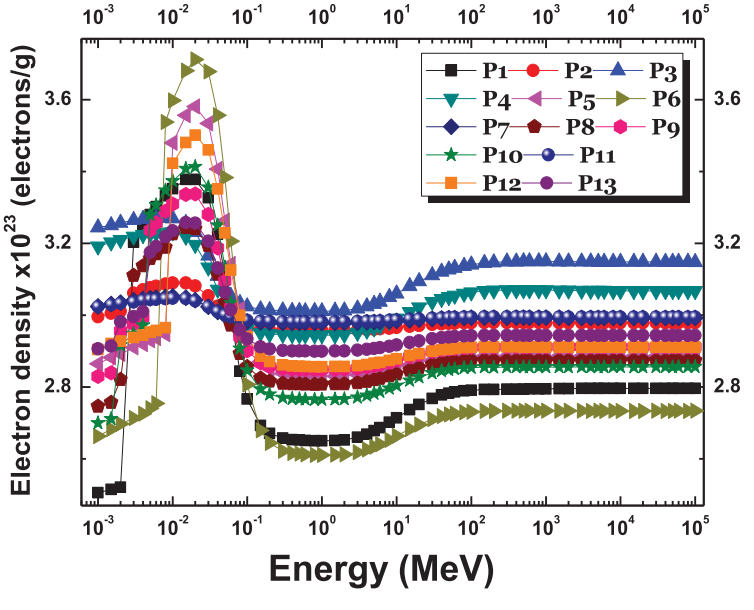

Figure 5. The variation in effective electron density of the polymers.

the sample. In addition, the P1 and P6 have maximum Z_{eff} value while the P3 has the lowest Z_{eff} value between 10 and 100 keV (Figure 4). The shielding ability of a sample is directly related to its Z_{eff} value. Due to their high Z_{eff} value and boron and iron contents, the P1 and P6 samples can be evaluated with the best shielding materials. Furthermore, the P3 sample appears as transparent materials for gamma radiations. The computed values of N_e for the extended energy range 0.015–15 MeV have been presented in Figure 5. The correlation between shielding and Z_{eff} must be confirmed in effective electron density (N_{eff}). Although

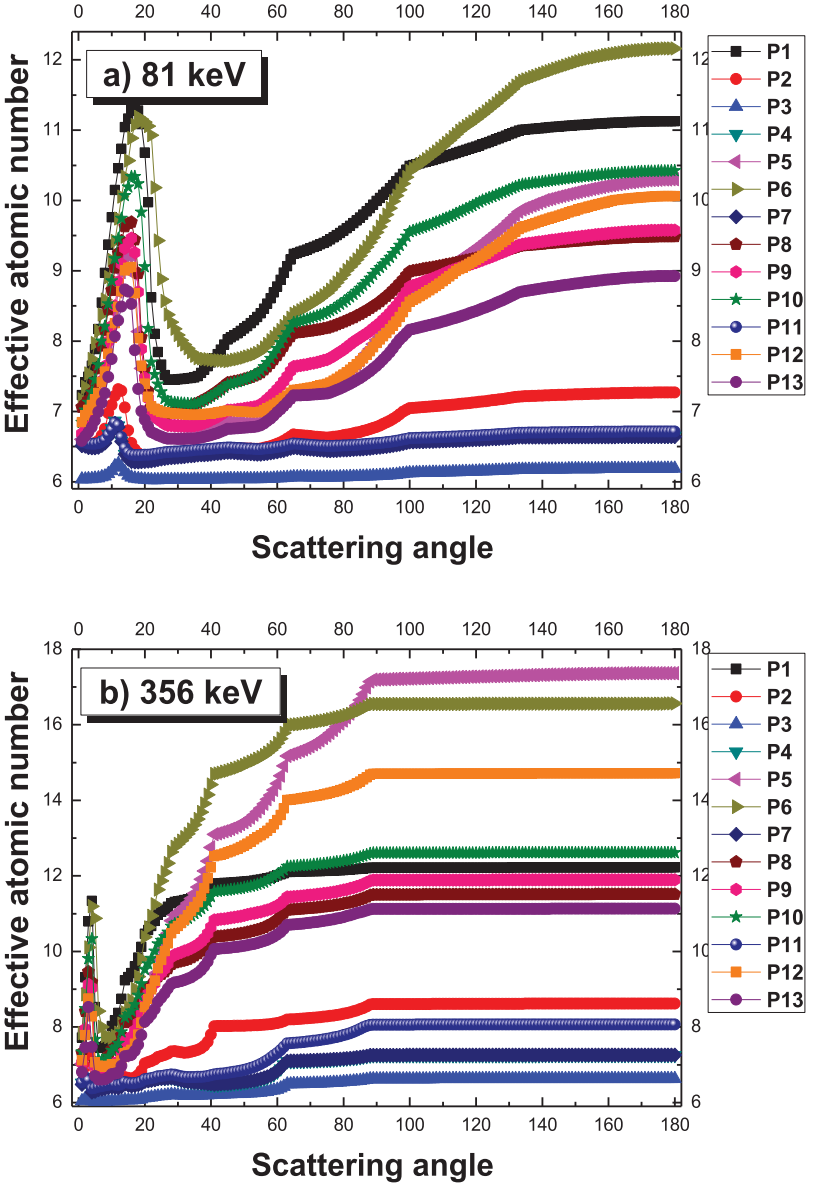

Figure 6. The variation in effective atomic numbers with scattering angles at 81 and 356 keV.

the P1 and P6 samples have minimum values of N_e, the P3 is lowest value in the selected energy range 10^{-1}–15 MeV.

Many researchers have assessed the Z_{eff} by uncompromised values for the incident energy and scattering angle (*21*, *22*). Yalçın et al. (*23*) have reported that a compromise between incident energy and scattering angle cannot be ignored by scientists calculating

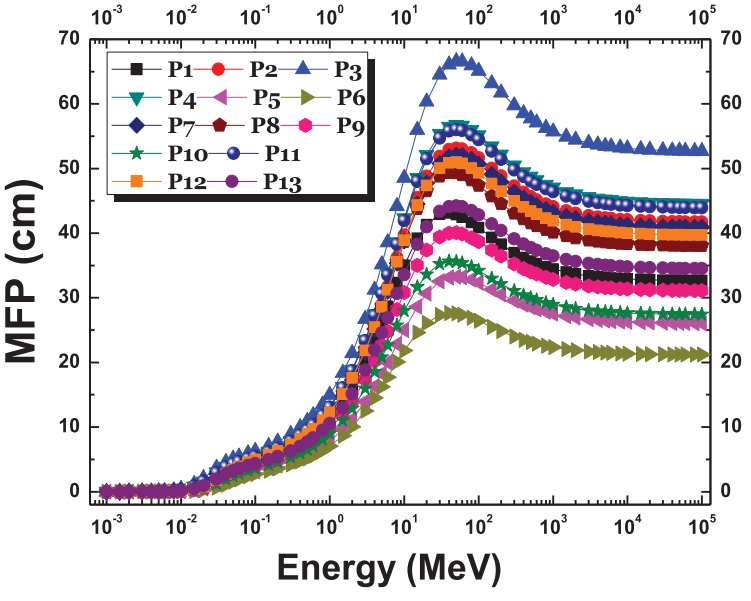

Figure 7. The variation in MFP of the polymers.

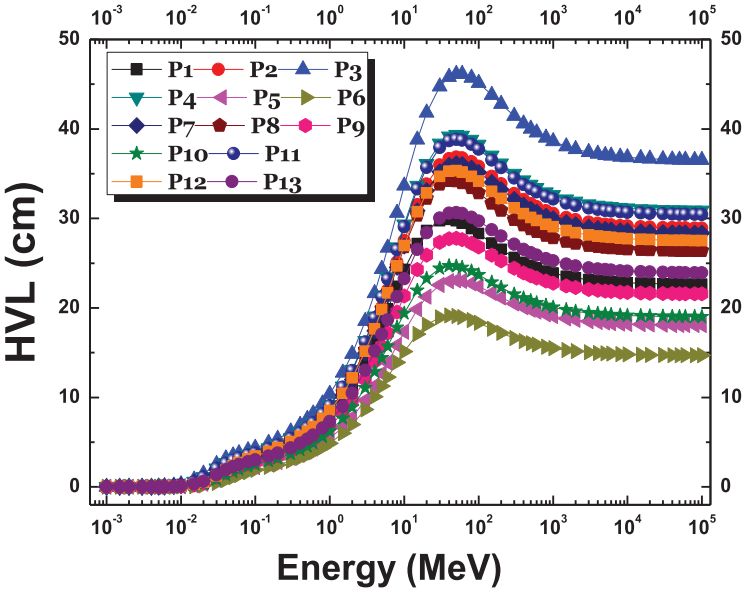

Figure 8. The variation in a half-value layer of the polymers.

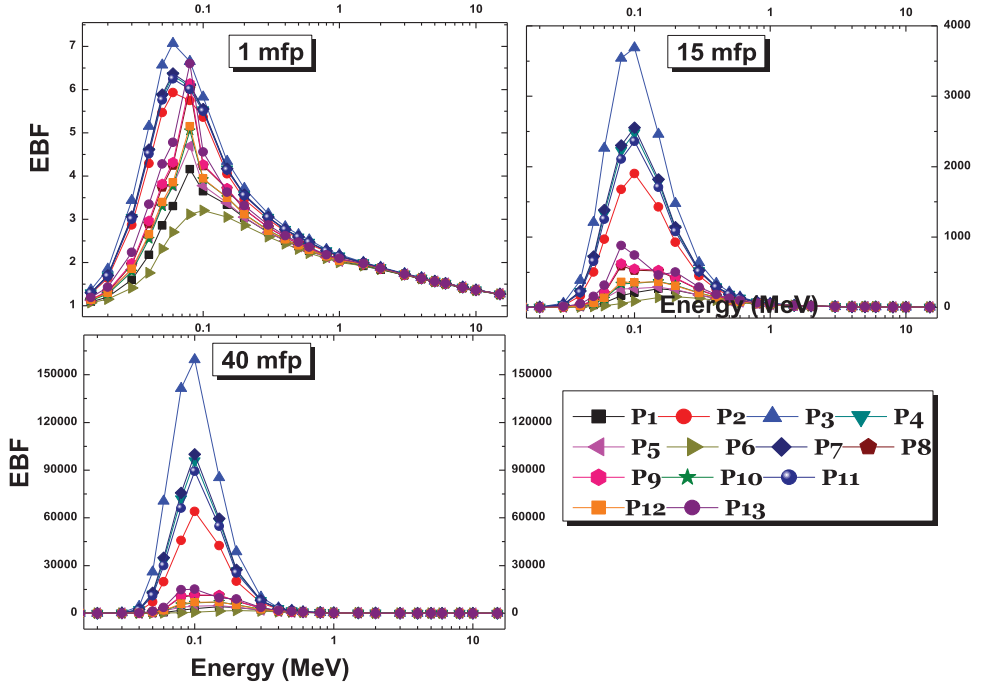

Figure 9. The variation in EBF with incident photon energy at 1, 15, and 40 MFP.

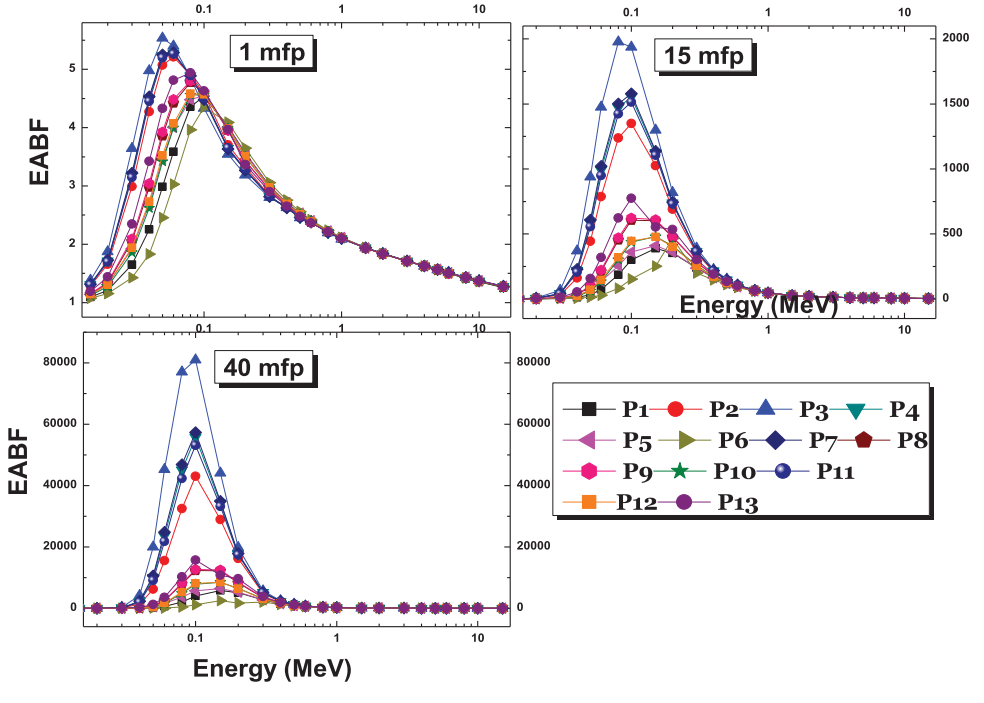

Figure 10. The variation in EABF with incident photon energy at 1, 15, and 40 MFP.

the Z_{eff} theoretically, experimentally, or with methods such as fit parameters. Figure 6 illustrates that scattering angle parameter cannot be negligible in calculating (Z_{eff}) especially at a small angle of 150°.

The computed results of the materials have been compared in terms of MFP with thirteen types of polymers and composites generally used for shielding applications as shown in Figure 7. It was seen that the P6 sample displayed the lowest MFP value as compared to the other samples. This result has confirmed that the P6 is appropriate material for shielding application. Figure 8 shows the change of HVL of the materials with the incident energy. An ideal shielding material must have a low HVL value. These values ascend with increasing photon energy as seen in Figure 8. In the low-energy region (<1 MeV), the values of HVL for all polymers and composites are very and fast increasing in HVL values can be noticed in this region. In the high-energy region (1 MeV $<$ E $<$ 5 MeV), it is observed that the HVL values of the present polymers increase gradually by increasing photon energy and become nearly constant in the high-energy region (E $>$ 100 MeV) (*24*).

Figures 9 and 10 show the variations in EBF and EABF with incident photon energy for the given samples at different penetration depths; 1, 15, and 40 MFP, respectively. From these graphics, it is clear that initially, the EBF and EABF values start increasing with the increase in photon energy and attain maximum values at intermediate energy region, then start decreasing with the further increase in photon energy up to 15.0 MeV. This can be clearly explained on the basis of the dominance of different partial photon interaction processes in various energy regions. Photoelectric effect is predominated in the low-energy region. The maximum number of photons are absorbed or removed, as EABF and EBF values show the minimum values. With an increase in incident photon energy, Compton scattering is the dominant process. It results in multiple Compton scattering events, which results in increasing EABF and EBF. In the high-energy region, a different absorption process, i.e. pair production starts to dominate which reduces EABF and EBF values. It is worth noting that all the materials showed almost similar variations in EBF and EABF in the continuous energy region based on the domination of different photon interaction processes in different energy regions. Based on these graphics, it has been observed that for all the selected polymers, the buildup factors were small at lower energies of the incident photon compared to higher energies of the incident photon. Additionally, maximum buildup factors were observed in the intermediate energy region. The factor accounts for the amount of forwarding scattering by the shield; B is a function of material and gamma-ray energy as well as geometry. The P6 polymer has the lowest EABF and EBF values due to high density.

5. Conclusion

In conclusion, the photon interaction properties of polymers and their composites have been examined at various photon energies using both experimental and MC based on transmission technique. The experimental results were compatible with MC and theoretical results according to mass attenuation coefficients. It was proposed that the polymer structures played important role in to the shielding properties against spatial low and high-energy radiation in the present study. Compared with a conventional passive shield, P1 and P6 exhibited better shielding capability, as indicated by lower amounts of effective electron density. The mass attenuation coefficient results have a similar tendency and display that the interaction possibility is highly relevant to the effective atomic number. The shielding

properties of P1 and P6 were affected by boron and iron contents. Within these polymers, the P1 and P6 had the most boron and iron elements, respectively. Among them, the P6 sample was recommended as better armor material than the other polymers.

It is verified that the ZXCOM can calculate the (Z_{eff}) at different energy and continuous scattering angle region for the polymers. Therefore, it was shown that a compatibility between incident energy and scattering angle was not ignored by scientists calculating the (Z_{eff}) experimentally or theoretically (*25*). This scattering parameter, which must be ignored in experimental measurements, contains 13 polymers included into ZXCOM program. The present practice of determination of the effective atomic number (Z_{eff}) and the effective electron density (N_{eff}) was not simple, but more reliable than the WinXCom which ignores the scattering angle.

Generally, the materials having low HVL and MFP values provide good shielding properties, therefore, the P6 polymer may be served as an alternative gamma-ray shielding material. Considering gamma-ray interaction parameters, such as mass attenuation coefficients, MFP, HVL, effective atomic number (Z_{eff}), the effective electron density (N_{eff}), and MCNP, the results confirmed that P6 and P1 own utmost shielding ability for gamma rays. Finally, the results show significant differences (between Max. and Min. values) among polymers under study for experimental results of MFP and HVL (up to around 59.68%).

Acknowledgements

The authors thank Eurotec engineering plastic company for supplying the samples.

Disclosure statement

No potential conflict of interest was reported by the authors.

ORCID

M. A. Taşdelen http://orcid.org/0000-0002-7012-7029

References

(1) Alkan, Ü.; Kılıç, M.; Karabul, Y.; Yamak, H.B.; Okutan, M.; İçelli, O. *J. Nanoelectron. Optoelectron*. **2016**, *11*, 343–348.
(2) Büyükyıldız, M. *Turkish J. Phys*. **2016**, *40*, 278–286.
(3) Kılıç, M.; Karabul, Y.; Alkan, Ü.; Yagci Ö.; Okutan, M.; Okutan, M.; Okutan, M.; İçelli, O. *Physicochem. Probl. Miner. Process*. **2017**, *53*, 578–590.
(4) Abdo, A.E.-S.; Ali, M.A.M.; Ismail, M.R. *Radiat. Phys. Chem*. **2003**, *66*, 185–195.
(5) Abdo, A.E.-S.; El-Sarraf, M.A.; Gaber, F.A. *Ann. Nucl. Energy*. **2003**, *30*, 175–187.
(6) Eid, G.A.; Kany, A.I.; El-Toony, M.M.; Bashter, I.I.; Gaber, F.A. *Arab J. Nucl. Sci. Appl*. **2013**, *46*, 226–233.
(7) Korkut, T.; Gencel, O.; Kam, E.; Brostow, W. *Int. J. Polym. Anal. Charact*. **2013**, *18*, 224–231.
(8) Aygün, B.; Korkut, T.; Karabulut, A.; Gencel, O.; Karabulut, A. *Int. J. Polym. Anal. Charact*. **2015**, *20* 323–329.
(9) AL-Dhuhaibat, M.J.R. *Int. J. Appl. or Innov. Eng. Manag*. **2015**, *4*, 90–98.
(10) Ambika, M.R.; Nagaiah, N.; Harish, V.; Lokanath, N.K.; Sridhar, M.A.; Renukappa, N.M.; Suman, S.K. *Radiat. Phys. Chem*. **2017**, *130*, 351–358.
(11) Sathiyaraj, P.; Samuel E.J.J.; Valeriano C.C.S.; Kurudirek, M. *Vacuum*. **2017**, *143*, 138–149.
(12) Kurudirek, M. J. *Alloys Comp*. **2017**, *727*, 1227–1236.
(13) Gerward, L.; Guilbert, N.; Jensen, K.B.; Levring, H. *Radiat. Phys. Chem*. **2004**, *71*, 653–654.

(14) Kurudirek, M.; Topcuoglu, S. *Nucl. Instruments Methods Phys. Res. Sect. B Beam Interact. with Mater. Atoms*. **2011**, *269*, 1071–1081.
(15) İçelli, O.; Mann, K.S.; Yalçın, Z.; Orak, S.; Karakaya, V. *Ann. Nucl. Energy*. **2013**, *55*, 341–350.
(16) Singh, V.P.; Badiger, N.M. *J. Radiol. Prot*. **2014**, *34*, 89–101.
(17) Karabul, Y.; Amon Susam, L.; İçelli, O.; Eyecioğlu, Ö. *Nucl. Instruments Methods Phys. Res. Sect. A Accel. Spectrometers, Detect. Assoc. Equip*. **2015**, *797*, 29–36.
(18) Eyecioglu, Ö.; Karabul, Y.; El-Khayatt, A.M.; İçelli, O. *Radiat.* Eff. *Defects Solids*. **2016**, *171*, 965–977.
(19) Metropolis, N. *Los Alamos Sci*. **1987**, *15*, 125–130.
(20) Mann, K.S.; Rani, A.; Heer, M.S. *Radiat. Phys. Chem*. **2015**, *106*, 247–254.
(21) Singh, M.P.; Sandhu, B.S.; Singh, B. *Phys. Scr*. **2007**, *76*, 281–286.
(22) Singh, M.P.; Sharma, A.; Singh, B.; Sandhu, B.S. *Radiat. Meas*. **2010**, *45*, 960–965.
(23) Yalçın, Z.; İçelli, O.; Okutan, M.; Boncukçuoğlu, R.; Artun, O.; Orak, S. *Nucl. Instruments Methods Phys. Res. Sect. A Accel. Spectrometers, Detect. Assoc. Equip*. **2012**, *686*, 43–47.
(24) Sayyed, M.I. *J. Alloys Compd*. **2017**, *695*, 3191–3197.
(25) Eyecioğlu, Ö.; El-Khayatt, A.M.; Karabul, Y.; İçelli, O. *Nucl. Sci. Tech*. **2017**, *28*, 63. doi:10.1007/s41365-017-0220-0.